DOI: 10.24874/ti.2064.11.25.02

Tribology in Industry

www.tribology.rs

RESEARCH

Stability Analysis of Cylindrical Journal Bearing with Different Textured Surface

Harinder Pal Singh[a,*], Niranjan Singh[b], R.K Awasthi[a]

[a]*Department of Mechanical Engineering, Sardar Beant Singh State University, Gurdaspur, Punjab, India,*
[b]*Department of Mechanical Engineering, Model Institute of Engineering & Technology, Jammu, India.*

Keywords:

Textured journal bearings
Newtonian lubricants
Transient motion
Instability trajectory

* Corresponding author:

Harinder Pal Singh
E-mail: harinderpal05@gmail.com

Received: 11 November 2025
Revised: 20 December 2025
Accepted: 12 February 2026

A B S T R A C T

The stability of hydrodynamic journal bearings is critically influenced by surface texture geometry, particularly dimple location and shape. This study investigates the effects of three dimple configurations (partially textured-1, partially textured-2, and fully textured) and three dimple shapes (spherical, triangular and kite) on bearing stability and transient response. A theoretical model is developed by solving the modified Reynolds equation, accounting for texture-induced perturbations in the fluid-film. The finite element method (FEM) is employed to evaluate stability parameters such as critical mass, threshold speed, and whirl frequency ratio and transient trajectories under disturbances. Results reveal that the partially textured-2 outperforms other bearing configurations, enhancing hydrodynamic pressure and damping. Compared to plain bearings, this configuration increases critical mass by 4.74%, and reduces whirl frequency ratio by 0.75% at a dimple depth of 0.14. Among dimple shapes, spherical-shaped textures exhibit superior stability due to their asymmetric pressure distribution. Trajectory analysis demonstrates that partially textured-2 bearings with spherical-shaped dimples show stable cycles and lower vibration amplitudes than triangular and kite shape bearing configurations. These findings provide valuable insights for optimizing surface textures to improve bearing stability in high-speed rotating machinery.

1. INTRODUCTION

The Journal bearings are critical components in rotating machinery, providing support and reducing friction between moving parts. However, their performance is often limited by instabilities such as oil whirl and whip, which can lead to excessive vibrations and even catastrophic failures [1]. To mitigate these issues, surface texturing in the form of micro-dimples has emerged as a capable technique to improve hydrodynamic lubrication and stability [2].

To effectively determine stability around equilibrium, linear analysis plays a vital role in the transient response analysis of journal bearings. This involves calculating stiffness and

damping coefficients through small perturbation techniques, which are crucial for predicting the linear transient response to minor disturbances. Swami et al. [3] have investigated the role of lubricant film dynamics with non-Newtonian lubricants, highlighting their impact on stability. Jain et al. [4] emphasized the importance of precise stiffness and damping coefficient calculations, as these directly influence the forces generated within the bearing due to minor journal displacements. Tieu and Qiu [5] compared stability contours derived from linear and non-linear bearing force models, demonstrating that non-linear effects significantly influence stability, often predicting lower critical speeds than linear models.

Das et al. [6] analyzed the stability of hydrodynamic journal bearings under micropolar lubrication, showing that micropolar fluid parameters significantly alter stability thresholds. Li et al. [7] performed transient analyses of rigid rotors supported by elliptical, offset elliptical, three-lobe, and four-lobe journal bearings, using fast Fourier transform techniques. Barrett et al. [8] developed a rapid method for computing the non-linear response of finite-length plain journal bearings, incorporating a finite-length correction factor to improve non-linear force predictions.

Kirk and Gunter [9] analyzed the stability and transient motion of plain journal bearings mounted on flexible, damped supports. Chandrawat and Sinhasan [10] studied the steady-state and transient performance of flexible shell journal bearings, evaluating the effects of eccentricity ratio, load, and flexibility. Jain et al. [11] investigated the transient response of journals supported on elastic bearings, analyzing how eccentricity ratio, load, and bearing stiffness influence dynamic behavior. Choy et al. [12] conducted a non-linear transient and frequency response analysis of hydrodynamic journal bearings under varying operating conditions. Sinhasan and Goyal [13] examined the transient behavior of circular journal bearings lubricated with non-Newtonian fluids, comparing results with Newtonian lubricants. Li [14] analyzed journal orbits in non-linear dynamic bearing systems, assessing the impact of different parameters on stability. Rao et al. [15] developed an analytical approach for evaluating dynamic coefficients and performing non-linear transient analysis of hydrodynamic journal bearings. Majumdar et al. [16] used a non-linear transient technique to study the stability of gas-lubricated journal bearings, recording journal center trajectories under varying conditions. Singh et al. [17] compared the motion trajectories of porous and solid journal bearings, concluding that porous bearings exhibit greater stability. Singh et al. [18] further studied the effect of radial clearance on stability parameters and motion trajectories, reporting that non-linear motion trajectories enhance stability margins compared to linear trajectories. Kushare et al. [19] investigated the non-linear transient behavior of worn three-lobe hybrid journal bearings, finding that wear defects severely impact stability.

Recent studies have extensively explored the impact of surface texturing on the tribological and dynamic performance of journal bearings. Researchers [20-36] have demonstrated that various texture shapes such as spherical, rectangular, trapezoidal, and compound dimples can enhance load capacity, reduce friction, and improve stability margins by altering the bearing's dynamic coefficients. Brizmer and Kligerman [37] suggested that textured bearings may enhance rotor stability, while Matele and Pandey [38] highlighted the influence of circular, square, and dense square textures on dynamic performance. Further investigations by Sharma et al. [39-41] and Yamada et al. [42] confirmed that chevron and triangular textures improve steady-state and dynamic characteristics, including stiffness and damping coefficients. Meng et al. [43] further showed that optimally designed compound textures enhance critical speeds, underscoring the importance of texture geometry in rotor-bearing system stability. Singh and Awasthi [44] investigated their impact on the dynamic stability of hydrodynamic two-lobe journal bearings. Byotra and Sharma [45] reviewed the performance of textured hydrodynamic journal bearings, focusing on the effects of various texture geometries such as axial grooves, waviness, and elliptical patterns on load capacity and friction reduction. Their

review also addressed lubricant selection, micro-texturing methods, cavitation and acoustic behavior, and emphasized the role of advanced computational techniques and further optimization for improving bearing efficiency. Gu et al. [46] presented a multi-objective adaptive texture optimization technique using a grey wolf optimizer for journal bearings. Their results showed that under transient operating conditions, the optimized square textures significantly improved tribological performance, boosting load capacity by up to 15.8%, reducing friction by up to 29.3%, and lowering energy waste by up to 50.4%. Meng et al. [47] analyzed the dynamic behavior of journal bearings with compound surface textures using a finite-difference model coupled with the CC-FFT method. Their findings demonstrated that optimally distributed compound textures significantly enhance bearing stability by increasing direct stiffness, reducing cross-coupled stiffness, and improving the critical rotor speed compared with simple textured and smooth bearings. Zare Mehrjardi et al. [48] studied cubic, cylindrical, and semi-ellipsoidal surface textures on noncircular two-lobe journal bearings using a modified Reynolds equation and FEM. The results showed that textures in high-pressure regions of lower lobe enhanced pressure, static performance, and stability, with cubic textures showing the strongest influence, followed by cylindrical and semi-ellipsoidal shapes.

This study investigates the influence of three dimple configurations (partially textured-1, partially textured-2, and fully textured) and three dimple shapes (spherical, triangular, and kite) on the stability and transient response of hydrodynamic journal bearings. While extensive research has demonstrated the benefits of surface texturing on steady-state performance, a systematic investigation of how texture location, geometry and depth collectively affect dynamic stability particularly critical mass, threshold speed, whirl frequency ratio, and transient journal trajectories remains limited in the literature. The present work addresses this gap by developing a theoretical model based on the modified Reynolds equation, solved using the FEM, to evaluate stability parameters and linear transient motion.

2. GOVERNING EQUATIONS

Figure 1 illustrates the geometric configuration of a journal bearing with surface texturing.

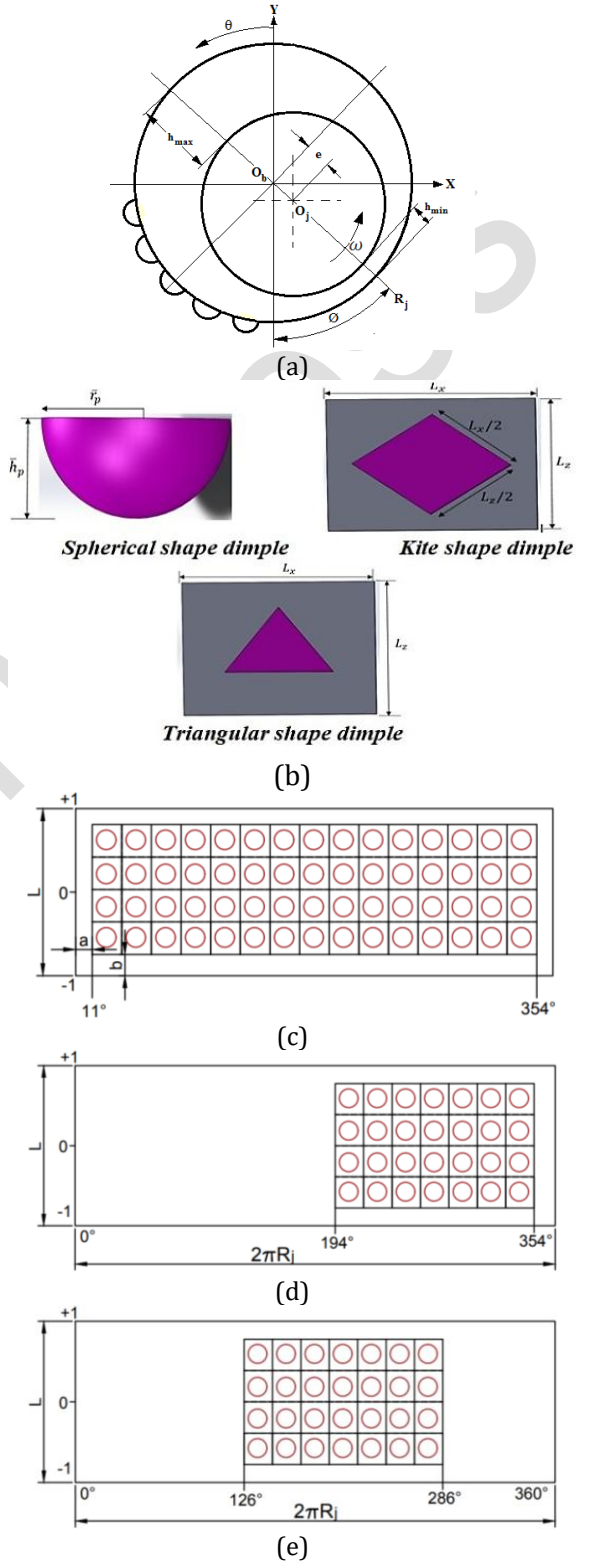

Fig. 1. (a) Journal bearing geometry with spherical textures, (b) various textures shapes, (c) Full textured bearing surface, (d) Partially textured-1 bearing surface (e) Partially textured-2 bearing surface.

The equations governing the laminar flow of an incompressible lubricant in the clearance space between the journal and the bearing can be written for journal centre motion trajectory in dimensionless form [14]

$$\frac{\partial}{\partial\alpha}\left(\frac{\bar{h}^3}{12}\frac{\partial\bar{p}}{\partial\alpha}\right)+\frac{\partial}{\partial\beta}\left(\bar{h}^3\frac{\partial\bar{p}}{\partial\beta}\right)=\frac{\Omega}{2}\frac{\partial\bar{h}}{\partial\alpha}+\frac{d\bar{h}}{d\bar{\tau}} \quad (1)$$

2.1 Lubricant- film thickness ($\bar{h}$)

The lubricant-film thickness of plain/ textured journal bearing can be written as

$$\bar{h}=\begin{Bmatrix}1-\bar{X}_j\cos\alpha-\bar{Z}_j\sin\alpha\\ 1-\bar{X}_j\cos\alpha-\bar{Z}_j\sin\alpha+\bar{h}_d\end{Bmatrix}\begin{matrix}\text{Plain bearing}\\ \text{Textured bearing}\end{matrix} \quad (2a)$$

Where, $\bar{X}_j$ and $\bar{Z}_j$ are the coordinates of centre, $\overline{X}_j=\varepsilon\sin\phi$, $\overline{Z}_j=-\varepsilon\cos\phi$

In the dimensionless form, the dimple depth ($\bar{h}_d$) of a spherically textured journal bearing can be written as [44].

When r $\leq \bar{r}_p$

$$\bar{h}_d=\left[\left(\frac{\bar{h}_p}{2}+\frac{\bar{r}_p^{\,2}}{2\bar{h}_p}\right)^2-\bar{r}_p^{\,2}(\bar{X}_L^{\,2}+\bar{Z}_L^{\,2})\right]^{1/2}-\left[\frac{\bar{r}_p^{\,2}}{2\bar{h}_p}-\frac{\bar{h}_p}{2}\right] \quad (2b)$$

When r $> \bar{r}_p$

$$\bar{h}_d=0 \quad (2b)$$

The expression of texture/dimple depth for triangular dimple can be written as

Triangular Texture ;

$$\bar{h}_d=\begin{Bmatrix}\bar{h}_p\ if\ (\bar{x}_l,\bar{z}_l)\notin\overline{\Omega}\\ 0\ if\ (\bar{x}_l,\bar{z}_l)\in\overline{\Omega}\end{Bmatrix}$$

$$\overline{\Omega}:\frac{-3}{4}\leq\bar{x}_l\frac{3}{4}\leq\bar{z}_l \text{ and}$$

$$-\frac{1}{\sqrt{3}}\leq\bar{x}_l-\frac{3}{4}\leq\bar{z}_l\leq\frac{1}{\sqrt{3}}\bar{x}_l+\frac{\sqrt{3}}{4} \quad (2c)$$

The expression of texture/dimple depth for kite shape texture can be written as
Kite Texture

$$\bar{h}_d=\begin{Bmatrix}\bar{h}_p\ if\ \bar{x}_l^{\,2}+\bar{z}_l^{\,2}<\bar{r}_p\\ 0\ if\ \bar{x}_l^{\,2}+\bar{z}_l^{\,2}>\bar{r}_p\end{Bmatrix} \quad (2d)$$

2.2 FEM formulation

The lubricant region is discretized using four-node quadrilateral iso-parametric elements. This discretization leads to a system of global linear equations governing the pressure field, which can be represented as [44].

$$[\bar{F}]_{N\times N}\{\bar{p}\}_{N\times1}=\{\bar{Q}\}_{N\times1}+\bar{\Omega}\{\bar{R}_H\}_{N\times1}+\dot{\bar{x}}\left\{\bar{R}_{X_j}\right\}_{N\times1}+\dot{\bar{z}}\left\{\bar{R}_{X_j}\right\}_{N\times1} \quad (3)$$

Where, N is number of nodes in the entire domain, involving the pressure $\{\overline{p}\}$ and the flow $\{\overline{Q}\}$ as nodal variables.

2.3. Boundary conditions

The following boundary conditions are used for calculating the influence of dimple location and shape on the stability and linear transient response of plain/partially textured journal bearings:

(i) The pressure is assume to be zero at the nodes lying on the external boundary of the bearing surface i.e. $\bar{p}=0$ at $\beta\pm1$.

(ii) The pressure gradient is assumed to be zero at the trailing edge of the positive region, $\frac{\partial\bar{p}}{\partial\alpha}=0$

(iii) The pressure is atmospheric at the leading edge, $\bar{p}=0$

Eq. (3) can be solved to give both pressure and flow simultaneously because at each node one of the two variables is known.

2.4. Stability parameters

Stability parameters of textured journal bearings are used to evaluate how surface texturing influences the dynamic stability of the rotor–bearing system. These parameters are derived from linearized dynamic coefficients of the bearing.

Critical mass ($\bar{M}_c$)

The critical mass is the maximum rotor mass that the bearing can support without instability. The non-dimensional value of critical mass ($\bar{M}_c$) of journal is given by [44]

$$\overline{M}_c = \frac{\overline{G}_1}{\overline{G}_2 - \overline{G}_3} \tag{4}$$

Where $\overline{G}_1 = \left[\overline{C}_{xx}\overline{C}_{zz} - \overline{C}_{zx}\overline{C}_{xz}\right]$

$$\overline{G}_2 = \frac{\left[\left(\overline{S}_{xx}\overline{S}_{zz} - \overline{S}_{zx}\overline{S}_{xz}\right)\left(\overline{C}_{xx} + \overline{C}_{zz}\right)\right]}{\left[\left(\overline{S}_{xx}\overline{C}_{zz} + \overline{S}_{zz}\overline{C}_{xx} - \overline{S}_{xz}\overline{C}_{zx} - \overline{S}_{zx}\overline{C}_{xz}\right)\right]}$$

$$\overline{G}_3 = \left[\frac{\left(\overline{S}_{xx}\overline{C}_{xx} + \overline{S}_{xz}\overline{C}_{xz} + \overline{S}_{zx}\overline{C}_{zx} + \overline{S}_{zz}\overline{C}_{zz}\right)}{\left(\overline{C}_{xx} + \overline{C}_{zz}\right)}\right]$$

Threshold speed($\overline{\omega}_{th}$)

The threshold speed is the rotational speed beyond which the system becomes unstable. It is calculated as [44]

$$\overline{\omega}_{th} = \left[\frac{\overline{M}_c}{\overline{F}_0}\right]^{\frac{1}{2}} \tag{5}$$

Where $\overline{F}_0$ is the fluid film reaction $\left(\frac{\partial \overline{h}}{\partial \overline{t}} = 0\right)$.

A journal bearing system is stable when the journal mass ($\overline{M}_j$) is less than the critical mass ($\overline{M}_c$). Similarly, when the operating speed of the journal is less than the threshold speed then the system is stable.

Whirl frequency ratio ($\overline{\omega}^2_{whirl}$)

Whirl frequency ratio is defined as the ratio of the oil-whirl frequency to the journal rotational frequency. Its higher value means poor stability and higher value means improved dynamic stability. Thus, reducing the whirl frequency ratio enhances the stability of a journal bearing. It can be expressed in non-dimensional form as [44]

$$\overline{\omega}^2_{whirl} = \left[\frac{K_1}{\overline{M}_c}\right] \tag{6}$$

$$K_1 = \frac{\overline{S}_{xx}\overline{C}_{zz} + \overline{S}_{zz}\overline{C}_{xx} - \overline{S}_{xz}\overline{C}_{zx} - \overline{S}_{zx}\overline{C}_{xz}}{\overline{C}_{xx} + \overline{C}_{zz}}$$

When the journal center is displaced from its static equilibrium position, it undergoes a variation in the hydrodynamic force. This results in a whirling motion of the journal around the equilibrium point due to the resulting unbalanced force. The corresponding motion trajectories are determined by numerically integrating the linearized equations of motion.

2.5. Linearized equations of motion

The equations governing the linearized motion of the journal are formulated as follows

$$\begin{bmatrix}\overline{M}_j & 0\\ 0 & \overline{M}_j\end{bmatrix}\begin{Bmatrix}\ddot{\overline{X}}\\ \ddot{\overline{Z}}\end{Bmatrix} + \begin{bmatrix}\overline{D}_{xx} & \overline{D}_{xz}\\ \overline{D}_{zx} & \overline{D}_{zz}\end{bmatrix}\begin{Bmatrix}\dot{\overline{X}}\\ \dot{\overline{Z}}\end{Bmatrix} + \begin{bmatrix}\overline{S}_{xx} & \overline{S}_{xz}\\ \overline{S}_{zx} & \overline{S}_{zz}\end{bmatrix}\begin{Bmatrix}\overline{X}\\ \overline{Z}\end{Bmatrix} = 0 \tag{7}$$

Equation (7) is solved numerically as an initial value problem using specified initial conditions for $\overline{x}$, $\overline{z}$, $\dot{\overline{x}}$, and journal mass $\overline{M}_j$, to determine the time-dependent responses The resulting trajectory traces the path of the journal center.

2.6. Modeling Assumptions and Limitations

The present study employs several established modelling assumptions common in hydrodynamic bearing analysis. The lubricant flow is modelled as isothermal, incompressible, and Newtonian, and the modified Reynolds boundary condition is applied to handle cavitation. This condition assumes film rupture occurs at ambient pressure and re-formation begins at the leading edge of the positive pressure zone. While this approach is computationally efficient and widely adopted for stability studies [44], it does not enforce mass conservation across the cavitation region. Consequently, the predicted positive pressure zone and resulting damping coefficients may be slightly overestimated, which could lead to a modest over prediction of stability margins. For applications requiring precise transient predictions under severe starvation or large disturbances, future work should incorporate mass-conserving cavitation models (e.g., Jakobsson–Floberg–Olsson). Furthermore, the model does not account for thermal effects, lubricant starvation, or surface elasticity, which may influence performance under high-speed or heavily loaded conditions. These limitations are acknowledged but are considered acceptable for the present comparative study focused on the relative effects of texture geometry on linearized stability and transient response.

3. NUMERICAL SOLUTION PROCEDURE

It is noticed in Fig. 2 that the load carrying capacity of textured journal bearing increases with the increase of number of elements in circumferential direction up to 63 and after 63 nearly stays constant. It is additionally observed from Fig. 3 that by increasing the number of elements in circumferential direction, the processing time increases gradually with no increment in load carrying capacity. Similar procedure is adopted for choosing the number of elements in axial direction and decided as 20. Therefore, to get work mesh independent and to limit computational time, the ideal mesh size has been chosen as 63 in circumferential direction and 20 in axial direction.

The numerical approach adopted in this study is presented in Fig. 4. Equation (3) is solved to obtain nodal pressure distributions and velocity components within the region of positive pressure in the lubricated domain. An iterative scheme is applied and continued until the solution converges within an acceptable tolerance. Once convergence is achieved, the resulting pressure field is used to compute the components of the hydrodynamic (fluid-film) force. To analyse the dynamic behavior, the journal's linear motion trajectories are computed by numerically integrating the linearized equations of motion (Eq. 7) using the classical fourth-order Runga-Kutta method. For this integration, appropriate initial conditions for $\overline{X}, \overline{Z}, \overline{\dot{X}}, \overline{\dot{Z}}$, along with a suitable time step, are specified to ensure accurate prediction of the journal centre's motion. At each time step, the film thickness is updated based on the current position and velocity values. This updated film thickness is then used to recalculate the fluid-film forces, which influence the motion in the subsequent step. This process is repeated iteratively over the entire time domain to trace the complete trajectory of the journal centre. It is noticed in figure 2 that the load carrying capacity of textured journal bearing increases with the increase of number of elements in circumferential direction up to 63 and after 63 nearly stays constant. It is additionally observed from figure 3 that by increasing the number of elements in circumferential direction, the processing time increases gradually with no increment in load carrying capacity. Similar procedure is adopted for choosing the number of elements in axial direction and decided as 20. Therefore, to get work mesh independent and to limit computational time, the ideal mesh size has been chosen as 63 in circumferential direction and 20 in axial direction.

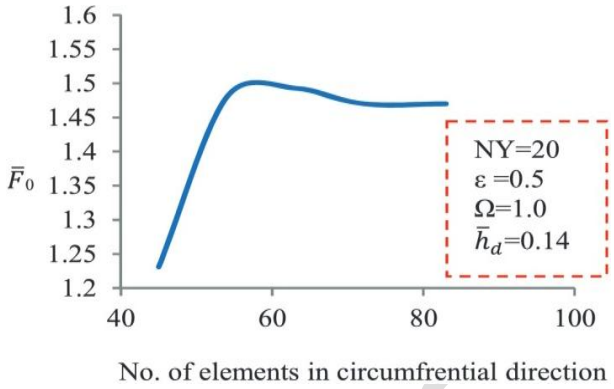

Fig. 2. Load carrying capacity versus number of elements in circumferential direction.

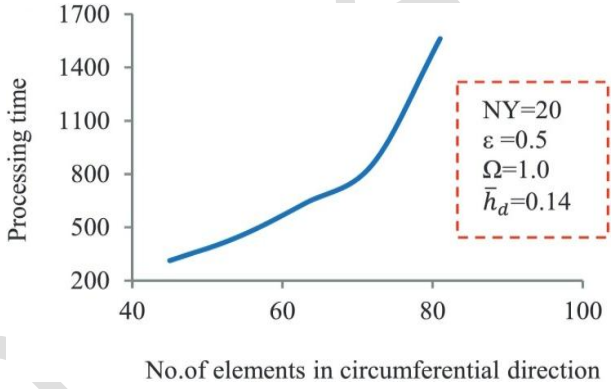

Fig. 3. Processing time versus number of elements in circumferential direction.

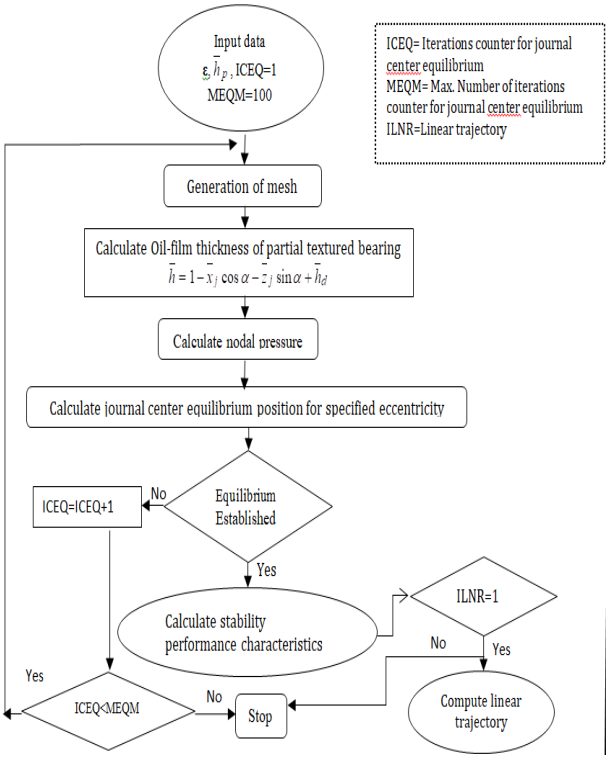

Fig. 4. Solution procedure for calculating the stability performance parameters and linear stability performance parameters and linear trajectory.

4. RESULTS AND DISCUSSION

4.1 Validation

In order to check the accuracy of the developed Matlab code for computing the stability parameters and the linear transient response of plan/textured journal bearings, the code is validated in two steps. In the first step, the computed dynamic characteristics of plain journal bearing are compared with the published work of Raimondi and Boyd [49], and Chandrawat and Sinhasan [50] as shown in Table 1. In the second step, the computed results of partially textured journal bearing are compared with the published work of Tala-Ighil [51] as shown in Table 2. The computed value appears to be in good agreement with the published work. To perform the current analysis, three different textured bearing configurations viz; full textured (11°-354°), partially textured-1(194°-254°) and partially textured-2 (126°-286°) and three different textures shapes such as spherical, triangular and kite shape are considered as shown in Fig.1. Table 3 presents the operating and geometric parameters used in this study, are selected from the published work of Singh and Awasthi [44].

Table 1. Comparison of dynamics characteristics of plain journal bearing (ε=0.6, L/D=1.0).

Performance parameters	1	2	3
$\bar{S}_{xx}$	1.9708	2.0	1.980
$\bar{S}_{zz}$	2.510	2.5	2.4860
$\bar{C}_{xx}$	2.23	2.2	2.7465
$\bar{C}_{zz}$	5.8446	5.75	5.9016

1. Present work
2. Raimondi and Boyd [49]
3. Chandrawat and Sinhasan [50]

Table 2. Comparison of statics characteristics of partially textured-II journal bearing (ε=0.6, L/D=1.0).

Performance parameters	Present work	Tala-Ighil [51]
Dimple depth $(\bar{h}_d)$	0.5	0.5
Angular location (θ)	185° –230°	185° –230°
Attitude angle (ϕ)	50.48	49.0
Max. pressure $(\bar{P}_{max})$	3.10	2.8

Table 3. Operating and geometric parameters used in the current work [44].

Parameters	Dimensionless values
Speed parameter (Ω)	1.0
Eccentricity ratio (ε)	0.3, 0.6
Clearance ratio (C_r)	0.001
Aspect ratio (L/D)	1.0
N_{cx}	7
N_{az}	4
No. of Nodes	1323
Area density of dimple(S_p)	50%
Texture radius ($\bar{r}_p$)	0.16
Texture depth ($\bar{h}_p$)	0.02- 0.14
a	0.2
b	0.2
L_x	2a
L_z	2b

4.2 Influence of dimple location on the stability of journal bearings

Three different textured bearing configurations viz; partially textured-1, partially textured-2 and full textured are used in order to investigate the influence of dimple location on the stability of journal bearings.

Influence on critical mass $(\overline{M}_c)$

Fig. 5 demonstrates the critical role of dimple location in governing the stability of textured journal bearings, quantified through the critical mass parameter as a function of dimple depth. The partially textured-2 (PT-2) configuration exhibits a prominent stability enhancement, manifested by an increase in critical mass with the increase of dimple depth. Similar kind of results are reported by Niranjan et al. [48]. This behavior stems from the PT-2's optimal dimple placement in pressure build-up regions, which enhances three key stabilizing mechanisms: (i) improved hydrodynamic pressure generation through controlled cavitation, (ii) improved lubricant entrainment via micro-reservoir effects, and (iii) enhanced damping through micro-vortices in the diverging zone. Therefore PT-2 bearings demonstrate superior suitability for high-speed rotor applications requiring whirl suppression. On the other hand both fully textured (FT) and partially textured-1 (PT-1) configurations show destabilizing tendencies, with critical mass reductions under identical dimple depth increments.

This deterioration arises from detrimental pressure field fragmentation in FT bearings and suboptimal dimple positioning in PT-1 designs that disrupt hydrodynamic wedge formation. For a specific dimple depth of 0.14 and eccentricity ratio of 0.3, the value of critical mass for PT-2 enhanced by an amount of 4.74% as compared to the plain bearing. The findings conclusively establish dimple location as the dominant design parameter over depth, with PT-2 bearing offering a wider stability margin compared to plain, fully textured and partially textured-1 bearings.

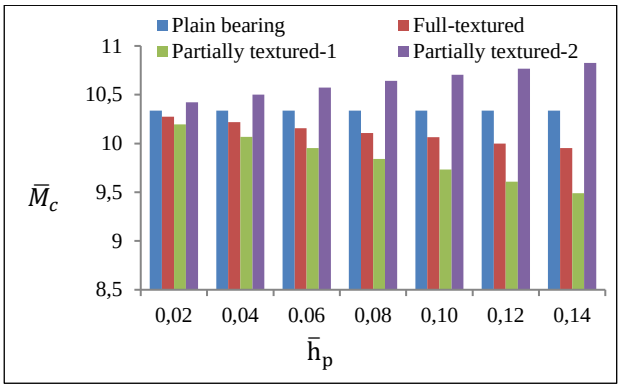

Fig. 5. Influence of dimple location on critical mass of journal ($\bar{M}_c$) versus dimple depth ($\bar{h}_p$).

Influence on threshold speed of stability ($\bar{\omega}_{th}$)

The stability characteristics of textured journal bearings exhibit significant dependence on dimple configuration, as evidenced by the threshold speed analysis presented in Fig. 6. For partially textured-2 (PT-2) bearing, the threshold speed of stability demonstrates a consistent reduction with increasing dimple depth. This destabilizing effect arises from the PT-2 configuration's specific dimple placement in pressure zones, where deeper dimples disrupt the optimal hydrodynamic pressure distribution and reduce fluid film stiffness. In contrast, both fully textured (FT) and partially textured-1 (PT-1) bearings show improved stability performance, with threshold speed increases over the same dimple depth range. The findings are consistent with those reported by Niranjan et al. [44] and Ramos et al. [52]. The enhanced stability in these configurations stems from more favourable pressure generation mechanisms. FT bearings benefit from uniform lubricant entrainment across the entire contact surface, while PT-1bearing achieves superior load capacity through strategically positioned dimples in primary load-bearing regions. These results demonstrate that while dimple depth influences stability characteristics, the specific dimple location represents the dominant factor in determining bearing performance.

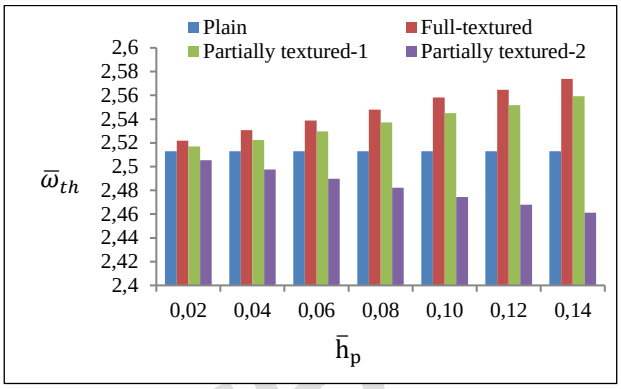

Fig. 6. Variation of threshold speed of stability ($\bar{\omega}_{th}$) versus dimple depth ($\bar{h}_p$).

Influence on whirl frequency ratio ($\bar{\omega}^2_{wirl}$)

The results presented in Fig. 7 demonstrate the critical influence of dimple location on the stability of textured journal bearings, as quantified by the whirl frequency ratio (WFR) across varying dimple depths. A lower $\bar{\omega}^2_{wirl}$ indicates greater stability, as it signifies a reduced tendency for the journal to enter a destabilizing whirling motion. Notably, the $\bar{\omega}^2_{wirl}$ of the partially textured-2 (PT-2) bearing decreases with increasing dimple depth, suggesting improved stability, whereas both the fully textured (FT) and partially textured-1 (PT-1) bearings exhibit an increase in $\bar{\omega}^2_{wirl}$, indicating diminished stability under the same conditions. Similar findings have also been reported by Singh et al. [44]. This contrasting behavior underscores the importance of dimple positioning in controlling bearing dynamics. The enhanced stability of PT-2 bearings can be attributed to the strategic placement of dimples within the pressure build-up region, which promotes more effective hydrodynamic pressure distribution, thereby suppressing whirl-inducing forces. These findings highlight that optimizing dimple location rather than merely increasing dimple depth is crucial for achieving superior bearing stability. This insight has significant practical implications for the design of high-performance bearing systems, particularly in applications where minimizing vibration and preventing unstable rotor motions are critical.

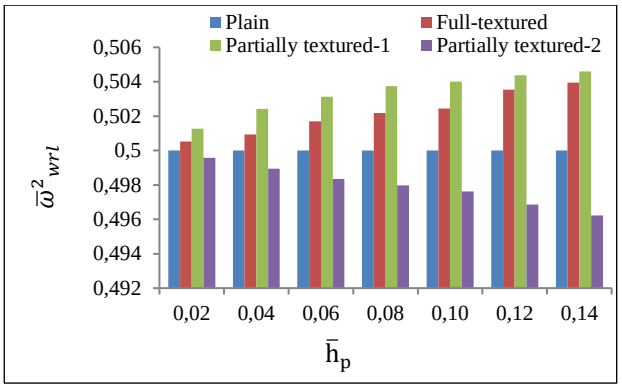

Fig.7. Variation of whirl frequency ratio $(\bar{\omega}^2_{wirl})$ versus dimple depth $(\bar{h}_p)$

4.3 Influence of dimple location on trajectory of journal bearings

The journal centre's motion trajectories are used to represent the transient response of both plain and textured journal bearing configurations. The initial values of displacements and velocities of the journal centre are set as $\bar{x} = \bar{z} = 0.05$ and $\dot{\bar{X}}$=$\dot{\bar{Z}}$=0.0 for all the bearing configurations studied. The motion trajectories are plotted at eccentricity ratio, ε=0.3 and dimple depth, $\bar{h}_p$ =0.14. The results indicate that the linearized equations of motion exhibit a limit cycle behavior when the journal mass is equal to the critical mass. In contrast, the journal undergoes unstable motion when its mass exceeds the critical value, and stable motion when the mass is below the critical threshold.

Fig. 8 illustrates the influence of dimple location on journal center motion trajectories, reflecting the dynamic stability of journal bearings at an eccentricity ratio of 0.3 and a dimple depth of 0.16. Under sub-critical mass conditions when the journal mass is less than the critical mass, all bearing types viz plain, partially textured-1, partially textured-2, and fully textured exhibit convergent spiral trajectories. This convergence signifies dynamic stability, where initial disturbances are gradually damped, leading to a stable operating state. Among the tested configurations, the partially textured-2 bearing demonstrates the optimal dynamic performance. This improvement is attributed to the strategic placement of dimples within the pressure build-up region (126°–286° circumferentially), covering the full axial length. These optimally located dimples generate localized hydrodynamic pressure zones that enhance load-carrying capacity and significantly improve damping. The result is increased film stiffness and better control of journal motion, which translates to reduced vibration amplitudes and greater system reliability. In comparison, the plain, partially textured-1, and fully textured bearings also exhibit stable behavior, but with slower convergence rates and larger final orbit sizes. These differences highlight the importance of dimple positioning in optimizing surface textures for superior dynamic stability in journal bearings under light mass conditions.

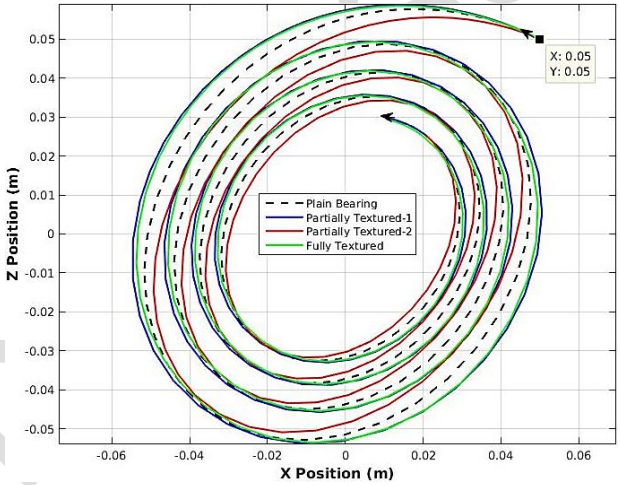

Fig. 8. The effect of dimple location on the trajectory of plain/textured journal bearings when $\bar{M}_j < \bar{M}_c$.

Fig. 9 illustrates the influence of dimple location on the dynamic behavior of journal bearings viz plain, partially textured-1, partially textured-2, and fully textured when the journal mass is equal to the critical mass. The trajectories represent the journal center's motion and exhibit limit cycle behavior, characterized by closed-loop orbits. Unlike the convergent spirals observed at sub-critical conditions, these sustained orbits indicate self-excited vibrations or whirl, reflecting operation at the stability threshold of the system. At this critical condition, the system does not return to a fixed equilibrium, but rather maintains a periodic motion in response to perturbations. Among the configurations, the partially textured-2 design shows a relatively smaller limit cycle, suggesting a better ability to control the amplitude of self-sustained oscillations. This performance is linked to the strategic placement of surface dimples in the pressure-generating zone, which enhances local hydrodynamic pressure and damping, even under borderline stability

conditions. Although all configurations exhibit limit cycle, the reduced orbit size in the partially textured-2 case indicates mitigated vibration severity, which can result in lower wear, noise, and improved operational reliability. This underscores the crucial role of optimized surface texturing in managing dynamic instabilities in journal bearings operating at critical mass.

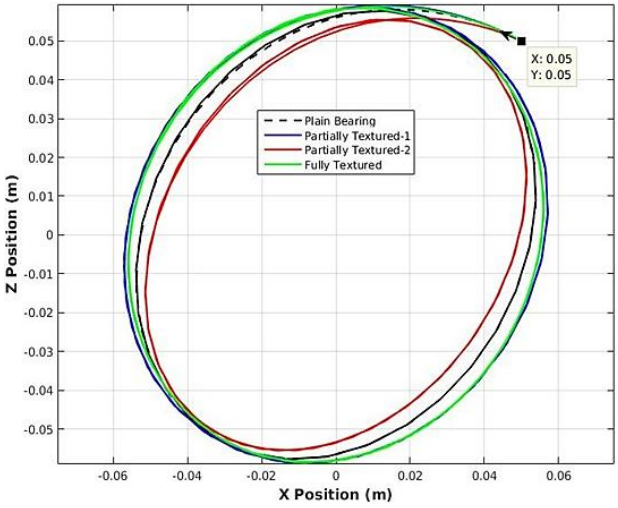

Fig. 9. The effect of dimple location on trajectory of plain/textured journal bearings when the $\bar{M}_j = \bar{M}_c$.

Fig. 10 illustrates the impact of dimple location on the dynamic stability of journal bearings under super-critical mass conditions (journal mass > critical mass). The trajectories depict diverging spiral orbits for all bearing configurations viz plain, partially textured-1, partially textured-2, and fully textured indicating unstable system behavior. In this regime, any initial disturbance grows with time, resulting in -increasing amplitude of journal motion. This divergence signifies that the inertia forces of the journal surpass the stabilizing effects of hydrodynamic pressure and damping, leading to self-excited vibrations, commonly referred to as oil whirl or oil whip. These instabilities pose serious reliability concerns, including elevated noise levels, excessive wear, metal-to-metal contact, premature bearing failure, and potential damage to associated rotating machinery. While complete instability is evident across all configurations, the rate and nature of the divergence vary. The plain bearing and partially textured-1 configurations show a more rapid outward spiral. In contrast, the partially textured-2 and fully textured bearings exhibit relatively tighter spiral paths for a longer duration before diverging, implying a delayed onset of instability. This suggests that although these surface textures cannot entirely stabilize the system at super-critical mass, they can provide enhanced damping and marginally delay failure. These results highlight the critical importance of surface texturing not only in promoting stability under normal operating conditions but also in moderating instability under adverse loading scenarios.

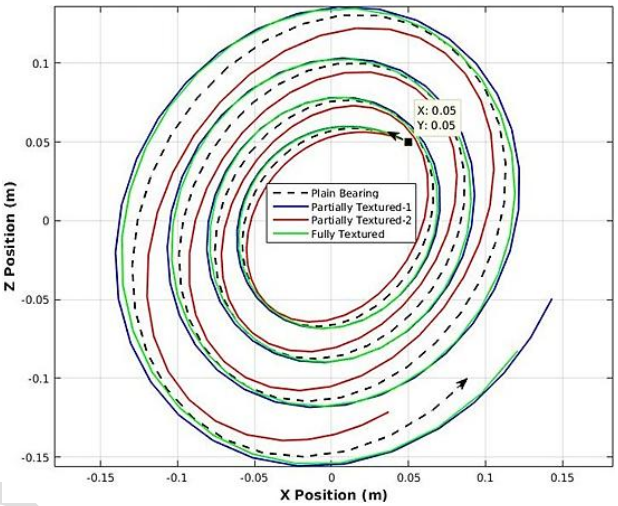

Fig. 10. The effect of dimple location on trajectory of plain/textured journal bearings when the $\bar{M}_j > \bar{M}_c$.

4.4 Influence of dimple shape on the stability of journal bearings

To examine the effect of dimple shape on the stability of journal bearing, the partially textured-2 bearing configuration is selected, as it demonstrated the optimal performance results as indicated prior analyses.

Influence on critical mass $(\overline{\mathrm{M}}_{\mathrm{c}})$

Fig. 11 shows the influence of different dimple shapes on the stability of journal bearings via critical mass as a function of dimple depth. Compared to plain bearings, all textured bearings improve stability by increasing the critical mass - the maximum load the bearing can support before becoming unstable. Spherical dimples give the biggest improvement (0.42% increase in critical mass), followed by kite-shaped (0.23%) and triangular-shaped (0.22%) patterns. Similar findings have also been reported by Singh et al. [44]. The stability of spherical textured bearing improves because these dimples can create better oil pressure distribution, which enhances the fluid film stiffness and damping capacity. This stronger

fluid-film can support heavier loads (higher critical mass) while maintaining stable operation. The findings provide practical guidance for engineers to select optimal texture shape when designing high-performance bearings that need to withstand heavy loads at high speeds.

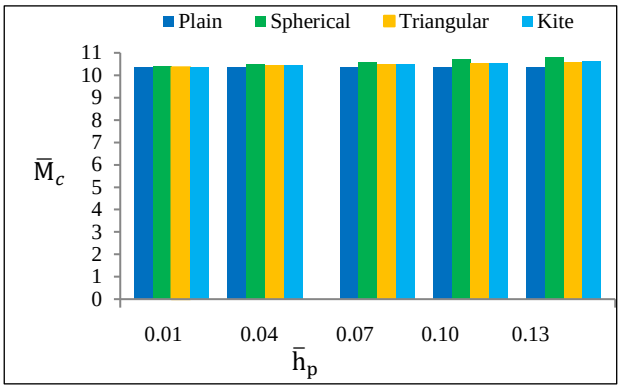

Fig. 11. Effect of dimple shape on critical mass $(\bar{M}_c)$ versus dimple depth $(\bar{h}_p)$

Influence on threshold speed of stability $(\bar{\omega}_{th})$

Fig. 12 illustrates the influence of dimple geometry (spherical, triangular, and kite-shaped) on the threshold speed of stability for textured journal bearings across a dimple depth range of 0.01–0.13. The results demonstrated a systematic reduction in threshold speed compared to plain bearing. Spherical dimples exhibited the most significant decline (0.18–2.11%), followed by triangular (0.08–1.10%) and kite-shaped (0.08–1.07%) bearing configurations. The findings are consistent with those reported by Singh et al. [44]. The results reveal a compromise between texture-enhanced performance (e.g., increased load capacity) and reduced stability, attributable to modified pressure distribution and altered stiffness/damping behavior. The spherical dimples' pronounced effect may arise from their symmetric geometry, which disrupts circumferential pressure gradients more uniformly than asymmetric shapes (triangular/kite). The marginally better stability retention of kite-shaped textures could be attributed to their streamlined profile, which minimally interferes with the lubricant's hydrodynamic wedge formation. These findings underscore the need for shape-specific optimization when designing textured bearings for stability-critical applications.

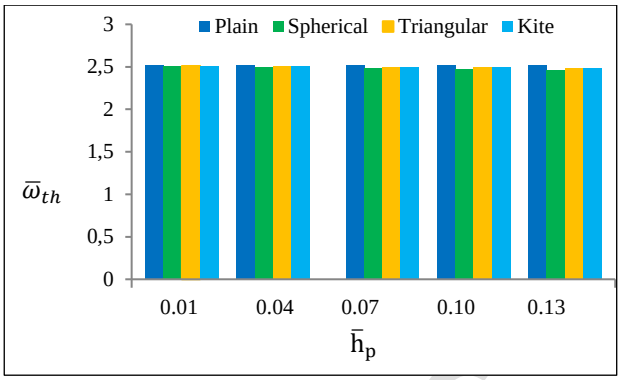

Fig. 12. Effect of dimple shape on threshold speed of stability $(\bar{\omega}_{th})$ versus dimple depth $(\bar{h}_p)$

Influence on whirl frequency ratio $(\bar{\omega}^2_{wirl})$

Fig. 13 presents the influence of dimple shape on bearing stability through whirl frequency ratio $(\bar{\omega}^2_{wirl})$ analysis across dimple depths of 0.01-0.13. The results demonstrate consistent $\bar{\omega}^2_{wirl}$ reductions in textured bearings compared to plain bearings, with the degree of improvement varying by both depth and geometry. Spherical dimples achieved the most significant stability enhancement (0.03-0.68% $\bar{\omega}^2_{wirl}$ reduction), outperforming both triangular (0.0-0.50%) and kite-shaped (0.0-0.54%) configurations. This $\bar{\omega}^2_{wirl}$ reduction directly correlates with improved stability, with spherical textures proving particularly effective due to their ability to optimize hydrodynamic pressure distribution and modify critical dynamic characteristics. The geometry-dependent performance variations emphasize the importance of strategic texture selection in bearing design, especially for high-speed applications where controlling whirl instability is paramount.

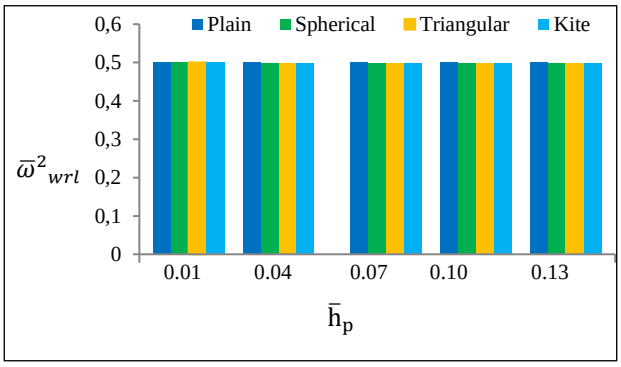

Fig. 13. Effect of dimple shape on whirl frequency ratio $(\bar{\omega}^2_{wirl})$ versus dimple depth $(\bar{h}_p)$

Fig. 14 illustrates the effect of dimple shape on the trajectories of journal bearings under conditions where the journal mass is less than the critical mass (CMF < 1). The trajectories for plain, spherical textured, triangular textured, and kite textured bearings all exhibit converging cycles, indicating a tendency toward stabilization. Notably, the spherical textured bearing demonstrates the smallest orbital radius among the tested configurations. This reduced radius signifies lower amplitude oscillations and faster convergence to equilibrium, highlighting the superior stability of spherical dimples. The enhanced stability can be attributed to the spherical dimple's uniform geometry, which promotes more effective lubrication film distribution and minimizes pressure fluctuations. In contrast, the triangular and kite textured bearings, with their asymmetric shapes, introduce localized disturbances in the lubricant flow, leading to larger orbital radii and slower stabilization. The trajectory analysis is critical as it directly correlates with the bearing's dynamic performance; smaller, convergent orbits imply reduced wear, lower energy dissipation, and prolonged operational life. These findings underscore the importance of dimple geometry optimization in designing high-stability journal bearings for precision applications.

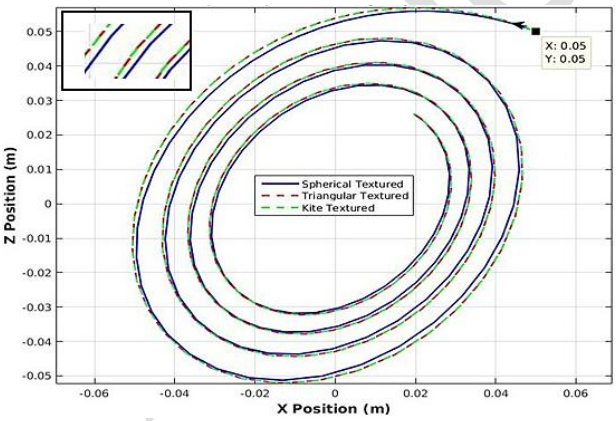

Fig.14. Effect of dimple shape on the trajectory of journal bearing when $\bar{M}_j < \bar{M}_c$.

Fig. 15 depicts the influence of dimple shape on the trajectories of journal bearings when the journal mass equals the critical mass (CMF = 1). The results reveal that all bearings spherical, triangular and kite textured bearings exhibit limit cycle behavior, indicating periodic oscillations under equilibrium conditions. However, the spherical textured bearing demonstrates the smallest orbital radius, suggesting superior stability compared to its counterparts. This enhanced stability arises from the spherical dimple's symmetrical geometry, which ensures uniform hydrodynamic pressure distribution and minimizes disruptive fluid vortices. In contrast, the triangular and kite textured bearings, due to their asymmetric designs, generate uneven pressure gradients, leading to larger orbital radii and less predictable motion. The trajectory's orbital radius is a critical indicator of dynamic stability, as smaller radii correlate with reduced vibration amplitudes, lower energy losses, and improved bearing longevity. These findings emphasize the significance of optimizing dimple geometry to enhance the stability and performance of journal bearings in high-precision mechanical systems, particularly under critical mass conditions.

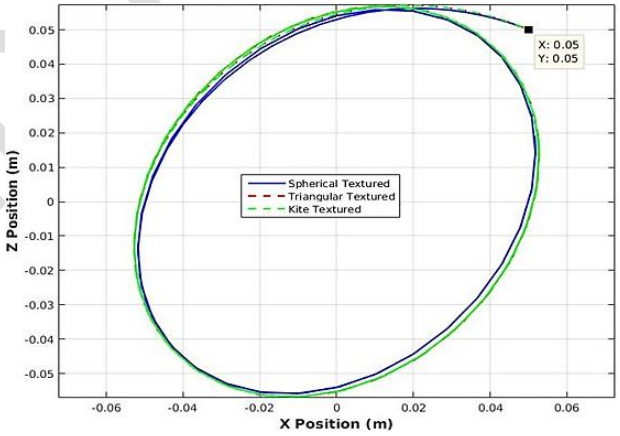

Fig.15. Effect of dimple shape on the trajectory journal bearing when $\bar{M}_j = \bar{M}_c$.

Fig. 16 demonstrates the dynamic behavior of journal bearings under conditions where the journal mass exceeds the critical mass, a situation commonly associated with hydrodynamic instability. As evidenced by the outward spiralling trajectories of all bearing types viz; plain, spherical, triangular, and kite-textured bearings —the system enters an unstable cycle. This instability is attributed to self-excited vibrations such as oil whirl or oil whip, where the hydrodynamic forces generated within the fluid-film become unstable, driving the journal into gradually larger orbits. Despite the overarching instability, the spherical textured bearing exhibits the least radius of

orbit among the tested configurations. This finding is significant because, while not achieving complete stability under these adverse conditions, a smaller orbital radius signifies a less severe form of instability. From a design perspective, a reduced orbital radius can delay the onset of bearing failure and mitigate wear even in systems prone to instability.

Table 4 presents the comparative analysis of different dimple shape influence on the stability parameters of journal bearings. It indicates that the stability of spherical textured journal bearing is significantly improved as compared to other textured bearings.

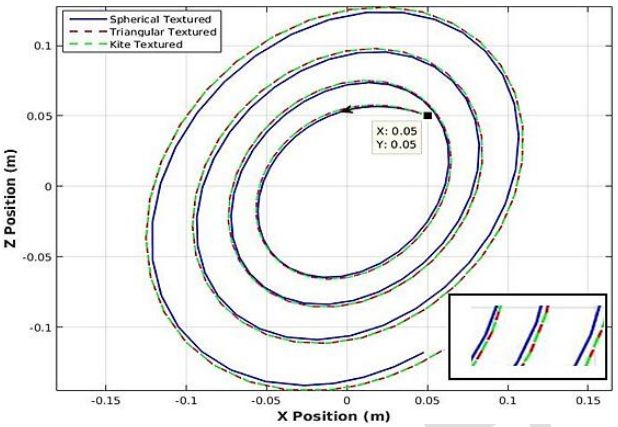

Fig.16. Effect of dimple shape on the trajectory of journal bearing when $\bar{M}_j > \bar{M}_c$.

Table.4. Influence of different dimple shape and depth on the stability performance parameters of textured journal bearing with respect to plain journal bearing.

BPPC	Dimple depth	Plain bearing	Spherical textured bearing	Triangular textured bearing	Kite textured bearing
$\bar{M}_c$ %change	$\bar{h}_p = 0.01$	10.336 0%	10.378 0.42%	10.359 0.22%	10.36 0.23%
	$\bar{h}_p = 0.13$	10.336 0%	10.78 4.30%	10.582 2.38%	10.604 2.59%
$\bar{\omega}_{th}$ %change	$\bar{h}_p = 0.01$	2.513 0%	2.50849 -0.18%	2.511 -0.08%	2.511 -0.08%
	$\bar{h}_p = 0.13$	2.513 0%	2.4599 -2.11%	2.4854 -1.10%	2.4861 -1.07%
$\bar{\omega}^2{}_{wrl}$ %change	$\bar{h}_p = 0.01$	0.5 0%	0.49987 -0.03%	0.5 0%	0.5 0%
	$\bar{h}_p = 0.13$	0.5 0%	0.4966 -0.68%	0.4975 -0.50%	0.4973 -0.54%

BPPC=$\left(\frac{TJB-PJB}{PJB}\right) \times 100$; BPPC= bearing performance parameter percentage change,
TJB= textured journal bearing, PJB=plain journal bearing.

4.5 Influence of dimple depth $(\bar{h}_p)$ on transient response of trajectory

The transient behavior of the plain and spherical textured journal bearing systems is illustrated through the motion trajectories of the journal center, as shown in Figures 15–17. For all cases analysed, the initial values of displacements and velocities of the journal centre are set as $\bar{x} = \bar{z} =$ 0.05 and $\dot{\bar{X}}$=$\dot{\bar{Z}}$=0.0. The motion trajectories are plotted at eccentricity ratio (ε=0.3) and for various values of dimple depth 0.01,007 and 0.13. The results reveal that the linearized equations of motion predict a limit cycle when the journal mass is equal to the critical mass. In contrast, unstable motion is observed when the journal mass exceeds the critical mass, while a stable response is achieved when the mass is below this threshold.

Fig. 17 presents the impact of dimple depth on spherical textured journal bearing trajectories when a journal mass below the critical mass ($\bar{M}_j$=0.9$\bar{M}_c$).The textured bearings exhibit converging spiral trajectory, indicating a stable operating condition. The lower journal mass contributes to this stability by reducing the dynamic forces acting on the bearing. The higher dimple depth enhances the stability of the bearing by increasing damping. The dimples can modify the lubricant film by creating localized pressure variations and enhancing lubricant flow. These changes in the lubricant film contribute to improved load-carrying capacity and reduced friction, leading to enhanced stability. These findings highlight the benefits of surface texturing to significantly enhance the stability of journal bearings operating under dynamic loads.

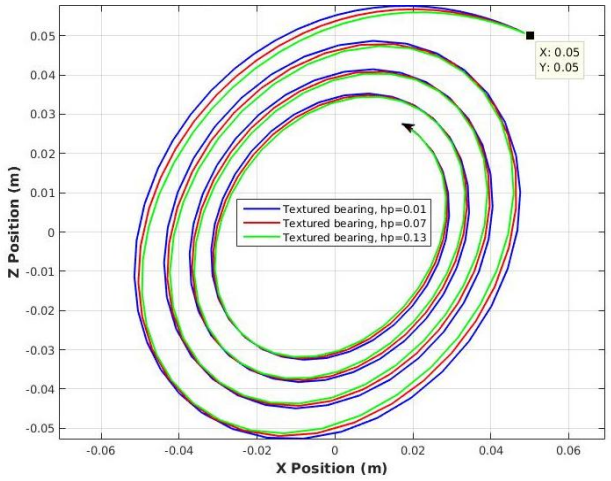

Fig. 17. Effect of dimple depth on trajectories of textured journal bearing when the $\bar{M}_j<\bar{M}_c$.

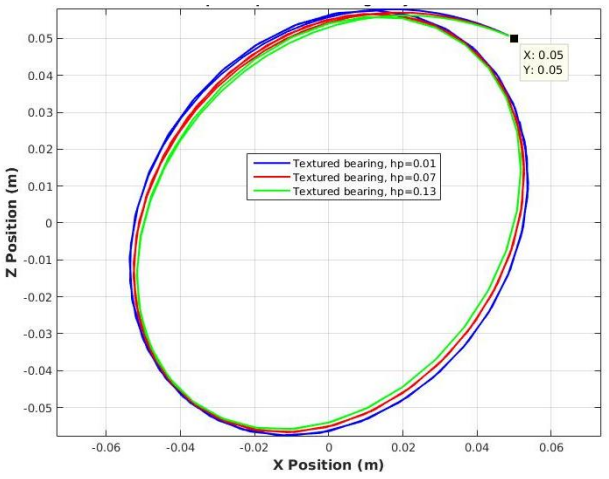

Fig. 18. Effect of dimple depth on trajectories of textured journal bearing when the $\bar{M}_j=\bar{M}_c$.

Fig. 18 illustrates the influence of dimple depth on the textured journal bearing trajectories when the journal mass equals the critical mass ($\bar{M}_j=\bar{M}_c$). The textured bearings exhibit limit cycle, and this amplitude of limit cycle further decreases with increasing dimple depth. This reduction in amplitude signifies enhanced stability, reduced vibration, and improved bearing performance**.** This observation can be attributed to the hydrodynamic effects induced by the dimples. These micro-dimples act as reservoirs for lubricant, influencing the pressure distribution within the bearing. As the dimple depth increases, the lubricant trapped within the dimples creates localized pressure variations. These pressure fluctuations alter the hydrodynamic forces acting on the journal, leading to a reduction in the amplitude of the limit cycle. The reduction in limit cycle amplitude observed in partial textured bearing at deeper dimple depth suggests improved stability and reduced vibration, which are critical factors for the reliable operation of high-speed rotating machinery.

Fig. 19 depicts the trajectories of textured journal bearings operating at an eccentricity ratio of 0.3 and various dimple depths. When the journal mass ($\bar{M}_j$) exceeds the critical mass ($\bar{M}_c$) i.e. ($\bar{M}_j$=1.2$\bar{M}_c$), the textured bearings exhibit unstable behavior, characterized by diverging spiral trajectories. This unstable behavior is expected as the system is operating beyond its stability threshold. However, a significant difference emerges between the bearing types: the deeper textured bearing demonstrates a slower rate of divergence compared to the other bearings.

Fig. 19 also demonstrates that surface texturing, particularly with increasing dimple depth, can significantly improve the robustness and reliability of journal bearings operating under unstable conditions. By influencing the lubricant dynamics, dimples contribute to a slower rate of divergence, mitigating the severity of instability.

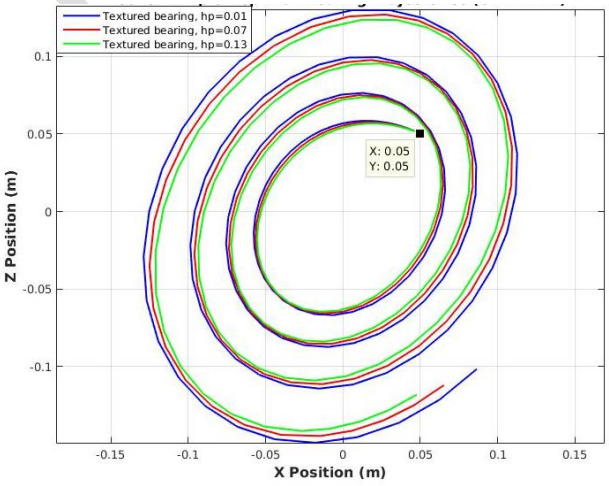

Fig. 19. Effect of dimple depth on trajectories of textured journal bearing when the $\bar{M}_j>\bar{M}_c$.

5. CONCLUSIONS

This comprehensive study evaluated the influence of dimple location and shape on bearing stability through critical mass, threshold speed, whirl frequency ratio, and transient trajectory analysis. Some important findings of this study are:

1. The partially textured-2 (PT-2) configuration, with dimples intentionally placed in the pressure build-up zone (126°–286°), significantly enhances bearing stability. This design improves hydrodynamic pressure distribution, damping, and lubricant entrainment, outperforming plain, fully textured (FT), and partially textured-1 (PT-1) bearings. Specifically, PT-2 increases critical mass by 4.74% and reduces the whirl frequency ratio by 0.75% at a dimple depth of 0.14, making it ideal for high-speed applications requiring robust stability.
2. Spherical dimples exhibit the optimum stability performance due to their symmetric geometry, which optimizes pressure distribution and enhances fluid film stiffness as compared to triangular and kite-shaped dimples.
3. Increasing dimple depth improves the stability, particularly for spherical dimples in the PT-2 configuration. Deeper dimples enhance damping and pressure generation, leading to faster convergence to equilibrium when journal mass is less than the journal critical mass and smaller limit cycles.
4. Textured bearings, especially PT-2 with spherical dimples, demonstrate superior transient response. When the journal mass is less than the critical mass, they exhibit faster convergence to equilibrium, while at critical mass, they produce smaller limit cycles. Even when journal mass is greater than the critical mass, textured bearings delay divergence, mitigating the severity of instability and prolonging bearing life.

Acknowledgement

We sincerely thank our institution for providing the facilities and technical support needed to carry out this research. The computational resources and laboratory infrastructure significantly contributed to the successful completion of this study.

REFERENCES

[1] D. W. Childs, *Turbomachinery Rotordynamics: Phenomena, Modeling, and analysis*, Wiley, 1993.

[2] I. Etsion, "State of the art in laser surface texturing," Journal of Tribology, vol. 127, no. 1, pp. 248–253, Jan. 2005, doi: 10.1115/1.1828070

[3] S. T. N. Swamy, B. S. Prabhu, and B. V. A. Rao, "Stiffness and damping characteristics of finite width journal bearings with a non-newtonian film and their application to instability prediction," *Wear*, vol. 32, no. 3, pp. 379–390, May 1975, doi: 10.1016/0043-1648(75)90324-5.

[4] S. Jain and L. Bajpai, "Analysis of Fluid Film Stiffness and Damping Coefficient for a Circular Journal Bearing with Micropolar Fluid," *International Journal on Emerging Technologies*, vol. 5, no. 1, pp. 206–211, Jan. 2014.

[5] A. K. Tieu and Z. L. Qiu, "Stability of finite journal bearings from linear and nonlinear bearing forces," *Tribology Transactions*, vol. 38, no. 3, pp. 627–635, Jan. 1995, doi: 10.1080/10402009508983452.

[6] S. Das, S. K. Guha, and A. K. Chattopadhyay, "Linear stability analysis of hydrodynamic journal bearings under micropolar lubrication," *Tribology International,* vol. 38, no. 5, pp. 500–507, May 2005, doi: 10.1016/j.triboint.2004.08.023.

[7] D.F. Li, K.C. Choy, and P.E. Allaire,"Stability and Transient Characteristics of Four Multilobe Journal Bearing Configurations," *Journal of Lubrication Technology*, vol. 102, no. 2, pp. 291–298, Jul. 1980, doi: 10.1115/1.3251514.

[8] L.E. Barrett, P.E. Allaire, and E.J.A. Gunter, "Finite Length Bearing Correction Factor for Short Bearing Theory," *Journal of Lubrication Technology*, vol. 102, no. 2, pp. 283–290, Jul. 1980, doi: 10.1115/1.3251508.

[9] R.G. Kirk and E.J. Gunter, "Stability and Transient Motion of a Plain Journal Mounted in Flexible Damped Supports," *Journal of Engineering for Industry*, vol. 98, no. 3, pp. 576–592, May 1976. doi: 10.1115/1.3438940.

[10] H.N. Chandrawat and R. Sinhasan, "A Study of Steady State and Transient Performance Characteristics of a Flexible Shell Journal Bearing," *Tribology Transactions*, vol. 21, no. 2, pp. 137–48, Jun. 1988, doi: 10.1016/0301-679X(88)90048-5.

[11] S.C. Jain, R. Sinhasan, and S.C. Pilli, "Transient Response of a Journal Supported on Elastic Bearings," *Tribology International*, vol. 23, no. 3, pp. 201–209, Jun. 1990, doi: 10.1016/0301-679X(90)90017-J.

[12] F.K. Choy, M.J. Braun, and Y. Hu, "Non-Linear Transient and Frequency Response Analysis of a Hydrodynamic Journal Bearing," *Journal of Tribology*, vol. 114, no. 3, pp. 448–454, Jul. 1992. doi: 10.1115/1.2920904.

[13] R. Sinhasan and K.C. Goyal, "Transient Response of a Circular Journal Bearing Lubricated with Non- Newtonian Lubricants," *Wear*, vol. 156, no. 2, pp. 385–399, Jun. 1992, doi: 10.1016/0043-1648(92)90230-6.

[14] X.K. Li, "An Analysis of Journal Orbits for Non-Linear Dynamic Bearing Systems," *Theoretical and Computational Fluid Dynamics*, vol. 13, no. 3, pp 209–230, Aug. 1999, doi: 10.1007/s001620050116.

[15] T.V.V.L.N. Rao, S. Biswas, H. Hirani, and K. Athre, "An Analytical Approach to Evaluate Dynamic Coefficients and Non-Linear Transient Analysis of a Hydrodynamic Journal Bearing," *Tribology Transactions*, vol. 43, no. 1, pp. 109–115, Jan. 2008, doi: 10.1080/10402000008982319.

[16] M.C. Majumdar and B.C. Majumdar, "Non-Linear Transient Analysis for an Externally Pressurized Porous Gas Journal Bearing," *Wear*, vol. 132, no.2, pp. 139–150, Jul. 1989, doi: 10.1016/0043-1648(89)90208-1.

[17] D.V. Singh, R. Sinhasan, and S.P. Tayal, "Theoretical Prediction of Journal Center Motion Trajectory," *Journal of Tribology*, vol. 98, no. 3, pp. 620–628, Oct. 1976, doi: 10.1115/1.3452950.

[18] N. Singh, R.K. Awasthi, D. Singh, and J. Singh,"Modeling and Simulation of Bearing Clearance Effects on Journal Center Motion Trajectories," *Materials Today: Proceedings*, vol. 5, pp. 17585–17596, Jan. 2018, doi: 10.1016/j.matpr.2018.06.076.

[19] P.B. Kushare, S.C. Sharma, and V.K. Matsagar, "A Study of Non-Linear Transient Behavior of Worn Out 3-Lobe Non-Recessed Journal Bearing," *Jurnal Tribologi*, vol. 40, no. 1, pp. 164–178, 2024.

[20] I. Etsion, Y. Kligerman, and G. Halperin, "Analytical and Experimental Investigation of Laser-Textured Mechanical Seal Faces," *Tribology Transactions*, vol. 42, pp. 511–516, Jan. 1999, doi: 10.1080/10402009908982248.

[21] X. Wang, K. Kato, K. Adachi, and K. Aizawa, "The Effect of Laser Texturing of SiC Surface on the Critical Load for the Transition of Water Lubrication Mode from Hydrodynamic to Mixed," *Tribology International*, vol. 34, no. 10, pp. 703–711, Oct. 2001, doi: 10.1016/S0301-679X(01)00063-9.

[22] R.B. Siripuram and L.S. Stephens, "Effect of Deterministic Asperity Geometry on Hydrodynamic Lubrication," *Journal of Tribology*, vol. 126, no. 3, pp. 527–534, Jun. 2004, doi: 10.1115/1.1715104.

[23] Y. Fu, Y. Ye, Y. Zhang, and L. Cai, "The Technology of Laser Honing Applied in Distinctively Improving the Lubrication of Frictional Units," Key Engineering Materials, vols. 202–203, pp. 265–270, Jun. 2001, doi: 10.4028/www.scientific.net/KEM.202-203.265.

[24] I. Etsion, "Improving Tribological Performance of Mechanical Components by Laser Surface Texturing," *Tribology Letters*, vol. 17, no. 4, pp. 733–737, Nov. 2004, doi: 10.1007/s11249-004-8081-1.

[25] C. Gao, L. Cai, and Q. Bi, "Micro Elastohydrodynamic Lubrication of Point Contacts with Co-Existence of Longitudinal and Transverse Roughness," *International Journal of Nonlinear Science and Numerical Simulation*, vol. 5, no. 2, pp. 67–73, Jun. 2004, doi: 10.1515/IJNSNS.2004.5.2.113.

[26] X. Wang, K. Adachi, K. Otsuka, and K. Kato, "Optimization of the Surface Texture for Silicon Carbide Sliding in Water," *Applied Surface Science*, vol. 253, pp. 1282–1286, Mar. 2006, doi: 10.1016/j.apsusc.2006.01.076.

[27] M. Suh, Y. Chae, S. Kim, T. Hinoi, and A. Kohyama, "Effect of Geometrical Parameters in Micro-Grooved Crosshatch Pattern Under Lubricated Sliding Friction," *Tribology International*, vol. 43, no. 8, pp. 1508–1517, Mar. 2010, doi: 10.1016/j.triboint.2010.02.012.

[28] M.B. Dobrica, M. Fillon, M.D. Pascovici, and T. Cicone, "Optimizing Surface Texture for Hydrodynamic Lubricated Contacts Using a Mass-Conserving Numerical Approach," *Proceedings of the Institution of Mechanical Engineers, Part J: Journal of Engineering Tribology*, vol. 224, pp.737–750, Jun. 2010, doi: 10.1243/13506501JET673.

[29] A.R. Gherca, P. Maspeyrot, M. Hajjam, and A. Fatu, "Influence of Texture Geometry on the Hydrodynamic Performances of Parallel Bearings," *Tribology Transactions*, vol. 56, no. 3, pp. 321–332, Dec. 2013, doi: 10.1080/10402004.2012.752550.

[30] F.M. Meng, R. Zhou, T. Davis, J. Cao, J.Q. Wang, D. Hua, et al., "Study on Effect of Dimples on Friction of Parallel Surfaces Under Different Sliding Conditions," *Applied Surface Science*, vol. 256, no. 9, pp. 2863–2875, Nov. 2010, doi: 10.1016/j.apsusc.2009.11.041.

[31] D.T. Ling, Z.P. Liu, S.W. Xiong, D. Grzina, J. Cao, J.Q. Wang, et al., "Surface Texturing of Drill Bits for Adhesion Reduction and Tool Life Enhancement," *Tribology Letters*, vol. 52, no. 1, pp. 113–122, Aug. 2013, doi: 10.1007/s11249-013-0198-7.

[32] J. Wang, Z. Han, H. Chen, and D. Chen, "Drag Reduction by Dimples on Surfaces in Plane–Plane Contact Lubrication," *Tribology Letters*, vol. 31, no. 3, pp. 159–166, Aug. 2008, doi: 10.1007/s11249-008-9348-8.

[33] S. Kango, R. Sharma, and R. Pandey, "Comparative Analysis of Textured and Grooved Hydrodynamic Journal Bearing," *Proceedings of the Institution of Mechanical Engineers, Part J: Journal of Engineering Tribology*, vol. 228, no.1, pp. 82–95, Aug. 2014, doi: 10.1177/1350650113499742.

[34] C. Shen and M.M. Khonsari, "Effect of Dimple's Internal Structure on Hydrodynamic Lubrication," *Tribology Letters*, vol. 52, no. 3, pp. 415–430, Oct. 2013, doi: 10.1007/s11249-013-0225-8.

[35] T.V.L.N. Rao, A.M.A. Rani, and T. Nagarajan, "Load Capacity of Partially Textured Journal Bearing with Trapezoidal Recess," *Applied Mechanical Materials*, vol. 315, pp. 830–834, Apr. 2013, doi: 10.4028/www.scientific.net/AMM.315.830 DOI link .

[36] F.M. Meng, L. Zhang, and Y. Liu, "Effect of Compound Dimple on Tribological Performances of Journal Bearing," *Tribology International*, vol. 91, pp. 99–110, Jul. 2015, doi: 10.1016/j.triboint.2015.06.030.

[37] V. Brizmer and Y. Kligerman, "A Laser Surface Textured Journal Bearing," *Journal of Tribology*, vol. 134, no. 3, Jun. 2012, doi: 10.1115/1.4006511.

[38] S. Matele and K. Pandey, "Effect of surface texturing on the dynamic characteristics of hydrodynamic journal bearing comprising concepts of green tribology," *Proceedings of the Institution of Mechanical Engineers Part J Journal of Engineering Tribology*, vol. 232, no. 11, pp. 1365–1376, Feb. 2018, doi: 10.1177/1350650117752611.

[39] S. Sharma, G. Jamwal, and R. K. Awasthi, "Enhancement of steady state performance of hydrodynamic journal bearing using chevron-shaped surface texture," *Proceedings of the Institution of Mechanical Engineers Part J Journal of Engineering Tribology*, vol. 233, no. 12, pp. 1833–1843, May 2019, doi: 10.1177/1350650119847369.

[40] S. Sharma, G. Jamwal, and R.K. Awasthi,"Numerical Study on Steady State Performance Enhancement of Partial Textured Hydrodynamic Journal Bearing," *Industrial Lubrication and Tribology*, vol. 71, no. 9, pp. 1055–1063, Jun.2019, doi: 10.1108/ILT-03-2019-0083.

[41] S. Sharma, G. Jamwal, and R. K. Awasthi, "Dynamic and stability performance improvement of the hydrodynamic bearing by using triangular-shaped textures," *Proceedings of the Institution of Mechanical Engineers Part J Journal of Engineering Tribology*, vol. 234, no. 9, pp. 1436–1451, Dec. 2019, doi: 10.1177/1350650119891513.

[42] H. Yamada, H. Taura, and S. Kaneko, "Numerical and Experimental Analyses of the Dynamic Characteristics of Journal Bearings with Square Dimples," *Journal of Tribology*, vol. 140, no. 1, Jun. 2017, doi: 10.1115/1.4037151.

[43] F. Meng, Y. Zhang, L. Su, H. Yu, and Y. Zheng, "Dynamic characteristics of compound textured journal bearing," *Proceedings of the Institution of Mechanical Engineers Part J Journal of Engineering Tribology*, vol. 235, no. 7, pp. 1312–1334, Aug. 2020, doi: 10.1177/1350650120951378.

[44] N. Singh and R.K. Awasthi, "Influence of Surface Textures on the Dynamic Stability and Performance Parameters of Hydrodynamic Two-Lobe Journal Bearings," *Proceedings of the Institution of Mechanical Engineers, Part J: Journal of Engineering Tribology*, vol. 236, no. 8, pp. 1589–1602, Dec. 2021, doi: 10.1177/13506501211070093.

[45] D. Byotra and S. Sharma, "A review on the performance of the textured Hydrodynamic Journal Bearing," *Springer Proceedings in Materials*, pp. 247–263, Jan. 2023, doi: 10.1007/978-981-99-3844-5_27.

[46] C. Gu, Y. Cui, & D. Zhang, "Research on the optimal design approach of the surface texture for journal bearings," *Lubricants*, vol.12, no. 4, p. 111, Mar. 2024, doi: 10.3390/lubricants12040111.

[47] F. Meng, Y. Zhang, L. Su, H. Yu, & Y. Zheng."Dynamic characteristics of compound textured journal bearing," *Proceedings of the Institution of Mechanical Engineers, Part J: Journal of Engineering Tribology*, vol. 235, no.7, pp. 1312-1334, Aug. 2021, doi: 10.1177/1350650120951378.

[48] M.Z Mehrjardi, A.R. Shooroki, A.D. Rahmatabadi and M.H. Mozaffari, "Effect of the geometric shape and position of surface textures on the dynamic stability of noncircular journal bearings," *Proceedings of the Institution of Mechanical Engineers, Part J: Journal of Engineering Tribology*, vol. 239 no. 12, pp. 1733-1750. May 2025, doi: 10.1177/13506501251335701.

[49] A.A. Raimondi and J. Boyd, "A Solution for the Finite Journal Bearings and Its Application to Analysis and Design, Parts I, II, III," *ASLE Transactions*, vol. 1, no. 1, pp. 194–209, Jan. 1958, doi: 10.1080/05698195808972330.

[50] H.N. Chandrawat and R. Sinhasan, "A Comparison Between Two Numerical Techniques for Hydrodynamic Journal Bearing Problems," *Wear*, vol. 119, pp. 77–87, Sep. 1987, doi: 10.1016/0043-1648(87)90099-8.

[51] N. Tala-Ighil, M. Fillon, and P. Maspeyrot, "Effect of Textured Area on the Performance of Hydrodynamic Journal Bearing," *Tribology International*, vol. 44, no. 3, pp. 211–219, oct. 2011, doi: 10.1016/j.triboint.2010.10.003.

[52] D. J. Ramos, L. I. Ramos, and G. B. Daniel, "Stability analysis of rotating systems supported by textured journal bearings," *Journal of Tribology*, vol. 142, no. 3, Oct. 2019, doi: 10.1115/1.4045191.

Nomenclature:

Dimensional parameters

C	Radial clearance, mm
C_{ij}	Lubricant-film damping coefficient (i, j=1,2)
D	Journal diameter, mm
E	Journal eccentricity, mm
H	Nominal thickness of lubricant-film, mm
h_p	Depth of dimple, mm
L	Length of bearing, mm
M_c	Journal critical mass (Kg)
M_j	Journal mass (Kg)
N	Speed of rotation, rpm
N_{az}	No. of textures in axial direction
N_{cx}	No. of textures in circumferential direction
O_B	Center of bearing
O_J	Center of journal
R_j, R_b	Radius of journal and bearing, mm
S_{ij}	Lubricant-film stiffness coefficient (i, j=1, 2)
T	Time, sec
X	Circumferential coordinate
Y	Axial coordinate
X, Z	Horizontal and vertical components of journal centre perturbation from its steady state equilibrium position
X_j, Z_j	Journal center coordinates

Greek Letters

μ	viscosity of Lubricant, Pa. sec
$\bar{\mu}_0$	Reference viscosity
θ	Textured portion
α	Angular co-ordinate in circumferential direction, radian
B	Angular coordinate in axial direction, radian
$\bar{\Omega}$	Angular speed, radian/sec
Φ	Attitude angle, radians

Subscripts and Superscript

b	Bearing
j	Journal
.	First derivative w.r.t. time
CMF	Critical mass factor

Dimensionless parameters

$$\bar{C}_{ij}=\left(\frac{c^3}{\mu_{R^4}{}_j}\right)C_{ij}$$

$$\bar{h},\bar{h}_{\min},\bar{h}_d=\left(\frac{h}{c},\frac{h_{\min}}{c},\frac{h_d}{c}\right)$$

$$\bar{M}_c=\frac{M_c}{\left[\mu_0 R^4/\omega c^3\right]}$$

$$\bar{M}_j=\frac{M_j}{\left[\mu_0 R^4/\omega c^3\right]}$$

$\bar{r}_p=\frac{r_p}{c}$, dimple radius

$$\bar{S}_{ij}=\left(\frac{c}{p_{sR^2}{}_j}\right)S_{ij}$$

$S_p=\frac{L_x\times L_z}{\pi\bar{r}_p{}^2}$, area density of dimple

$$\bar{X}_j,\bar{Z}_j=\left(\frac{X_j}{c},\frac{Z_j}{c}\right)$$

$$\bar{X},\bar{Z}=\left(\frac{X}{c},\frac{Z}{c}\right)$$

$$\alpha,\beta=\left(\frac{x}{R_j},\frac{y}{R_j}\right)$$

$$\varepsilon=\frac{e}{c}$$

$$\bar{\Omega}=\omega_j\left(\frac{\mu_r R_j{}^2}{c^2 p_s}\right)$$

$$\bar{X},\bar{Z}=(X,Z)/c$$

$$\dot{X},\dot{Z}=\frac{\left(\partial X/\partial t\right)}{\omega c},\frac{\left(\partial Z/\partial t\right)}{\omega c}$$

$$\ddot{X},\ddot{Z}=\frac{\left(\partial^2 X/\partial t^2\right)}{\omega^2 c},\frac{\left(\partial^2 Z/\partial t^2\right)}{\omega^2 c}$$

Matrices

$[\bar{F}]$= Assembled lubricant flow matrix
$\{\bar{P}\}$= Vector of nodal pressure
$\{\bar{Q}\}$= Vector of nodal flow
$\{\bar{R}_H\}$ = hydrodynamic terms column vectors
$\bar{R}_{Zj}$ = journal center linear velocities Global right hand side vectors